

Main Manuscript for

Orbitofrontal Cortex Modulates Auditory Cortical Sensitivity and Sound Perception

Matheus Macedo-Lima, Lashaka Sierra Hamlette, Melissa L. Caras
Department of Biology, University of Maryland, College Park

*Melissa L. Caras

Email: mcaras@umd.edu

Author Contributions: MML, LSH and MLC designed research; MML and LSH performed research; MML analyzed data; MML and MLC wrote the paper.

Competing Interest Statement: The authors declare no conflict of interest.

Classification: Biological Sciences; Neuroscience

Keywords: Attention; prefrontal cortex; top-down; cortical plasticity; behavioral context

This PDF file includes:

Main Text

Figures 1 to 5

Tables 1 to 1

1 **Abstract**

2 Sensory perception is dynamic, quickly adapting to sudden shifts in environmental or behavioral
3 context. Though decades of work have established that these dynamics are mediated by rapid
4 fluctuations in sensory cortical activity, we have a limited understanding of the brain regions and
5 pathways that orchestrate these changes. Neurons in the orbitofrontal cortex (OFC) encode
6 contextual information, and recent data suggest that some of these signals are transmitted to
7 sensory cortices. Whether and how these signals shape sensory encoding and perceptual
8 sensitivity remains uncertain. Here, we asked whether the OFC mediates context-dependent
9 changes in auditory cortical sensitivity and sound perception by monitoring and manipulating OFC
10 activity in freely moving animals under two behavioral contexts: passive sound exposure and
11 engagement in an amplitude modulation (AM) detection task. We found that the majority of OFC
12 neurons, including the specific subset that innervate the auditory cortex, were strongly modulated
13 by task engagement. Pharmacological inactivation of the OFC prevented rapid context-dependent
14 changes in auditory cortical firing, and significantly impaired behavioral AM detection. Our findings
15 suggest that contextual information from the OFC mediates rapid plasticity in the auditory cortex
16 and facilitates the perception of behaviorally relevant sounds.

17 **Significance Statement**

18 Sensory perception depends on the context in which stimuli are presented. For example, perception
19 is enhanced when stimuli are informative, such as when they are important to solve a task.
20 Perceptual enhancements result from an increase in the sensitivity of sensory cortical neurons;
21 however, we do not fully understand how such changes are initiated in the brain. Here, we tested
22 the role of the orbitofrontal cortex (OFC) in controlling auditory cortical sensitivity and sound
23 perception. We found that OFC neurons change their activity when animals perform a sound
24 detection task. Inactivating OFC impairs sound detection and prevents task-dependent increases
25 in auditory cortical sensitivity. Our findings suggest that the OFC controls contextual modulations
26 of the auditory cortex and sound perception.

27 **Main Text**

28 **Introduction**

29 Sensory perception is highly flexible, constantly adjusting to context-dependent changes in
30 arousal (1–4), attention (5, 6), or expectations about upcoming events (7–12). This rapid flexibility
31 favors the detection of important or informative stimuli, supporting improved communication,
32 predator avoidance, and reproductive success.

33

34 Context-dependent shifts in perception are thought to result from rapid changes in sensory
35 cortical processing. For instance, when a stimulus suddenly acquires behavioral relevance (such
36 as when it must be used to solve a task), sensory cortical neurons quickly adjust their tuning
37 properties, response strengths, and/or functional connectivity to optimize its detection,
38 discrimination, or identification (6, 13–31). These data indicate that sensory cortices must receive
39 signals that tell them when and how to adjust their activity, but where and how such signals are
40 initiated remains unclear.

41

42 Several lines of evidence suggest that the orbitofrontal cortex (OFC) is particularly well-
43 positioned to mediate contextual signaling. First, OFC is unique in that it is the only frontal cortical
44 region to integrate inputs from all sensory modalities (32, 33), providing it a distinct vantage point
45 for discerning shifts in environmental or behavioral demands. Second, in addition to their well-
46 established role in encoding value (34), OFC neurons also encode social (35), spatial (36, 37), and
47 behavioral context (38–41). While recent work indicates that some of these signals are transmitted
48 to sensory cortices (38–41), their downstream impact on sensory encoding and perceptual
49 sensitivity is only beginning to be understood.

50

51 Here, we asked whether OFC shapes sound processing and perception by relaying contextual
52 information to the auditory cortex in freely moving animals. We first recorded extracellular activity
53 from OFC neurons under two different behavioral contexts: passive sound exposure and
54 engagement in a sound detection task. We found that the majority of OFC neurons, including the
55 specific subset that innervate the auditory cortex, exhibited context-dependent changes in firing
56 rates. We then pharmacologically suppressed OFC activity during task engagement and assessed
57 the effect on auditory perception and auditory cortical sound processing. OFC inactivation both
58 impaired behavioral sound detection and prevented task-dependent changes of auditory cortical
59 firing. Our findings suggest that the OFC supports context-dependent modulations of stimulus
60 representations within the auditory cortex, contributing to the enhanced perception of behaviorally
61 relevant sounds.

62 **Results**

63 *OFC neurons are sensitive to behavioral context*

64 Auditory cortical neurons are more sensitive to amplitude-modulated (AM) stimuli when animals
65 perform an AM detection task compared to when the same sounds are presented in a passive,
66 non-task context (13). This finding, which is consistent with decades of work (17, 18, 20, 22, 23,
67 27, 28, 42–46), suggests that task engagement recruits non-sensory networks that modulate

68 auditory cortical response properties. If OFC participates in this process, then we should also
69 observe a neural signature of task engagement in OFC neurons.

70

71 To test this prediction, we trained Mongolian gerbils on the same AM detection task described
72 above. In this task, animals must drink from a waterspout in the presence of unmodulated noise
73 and withdraw from the spout when the sound transitions to an AM noise to avoid an aversive shock
74 (Figure 1A). Animals learned the task quickly, reaching expert performance levels ($d' \geq 2$, see
75 Materials and Methods) within ~250 trials across six sessions (Figure 1B-C; $n = 16$ animals across
76 all experiments). We then implanted five of these animals (two female) with 64-channel silicon
77 probe arrays in left OFC and recorded from 298 single- and 227 multi-units during task engagement
78 and during passive sound exposure sessions just before ('passive-pre') and just after ('passive-
79 post') the task (Figure 2A-C). During passive exposure sessions, the spout was removed from the
80 test arena and the shocker was turned off, but everything else, including the sound stimuli and
81 position of the recording electrodes, remained identical to the task.

82

83 We first examined the effect of task engagement on OFC activity during the presentation of AM
84 stimuli. During passive exposure sessions, OFC firing was unremarkable, with no obvious change
85 evoked by AM sounds. During task engagement, on the other hand, OFC neurons exhibited a
86 heterogenous array of responses (Figure S1). While some of these neurons may have been
87 sensitive to the AM stimulus, the majority appeared to be more sensitive to behavioral outcome,
88 with changes in firing sometimes lasting 2-4 seconds after AM onset. To verify whether the OFC
89 neurons that innervate auditory cortex exhibit similar dynamics, we injected a virus into the left
90 auditory cortex to retrogradely express the calcium indicator jRCaMP1e and implanted an optical
91 fiber into the left OFC ($n = 9$; four females). We found that during passive sound exposure, calcium
92 transients were largely absent. However, during task engagement, calcium transients were robust
93 and sensitive to behavioral outcome (Figure S2). These findings, which are broadly consistent with
94 prior work (38, 40, 41, 47) confirm that OFC neurons, including the subset of OFC neurons that
95 project to auditory cortex, encode behaviorally relevant information during task engagement.

96

97 We next examined the effect of behavioral context on the firing rates of OFC units during
98 periods of unmodulated noise presentation. We found that most units recorded (397/525; 76%)
99 were significantly modulated by context. Overall, 200/525 units (38%) were 'task-enhanced',
100 exhibiting elevated firing rates during the task compared to the initial passive-pre session (Figure
101 2D; Wilcoxon rank-sum test for each unit; see Supplementary Methods in SI Appendix). A roughly
102 equal number (197/525; 38%) were 'task-suppressed'. A smooth continuum of context-dependent
103 modulation was clearly observed (Figure 2E), similar to previous reports in the auditory cortex (48).
104 Moreover, the magnitude of the context modulation was largely similar between task-enhanced and
105 -suppressed units ($p = 0.207$; Figure 2F).

106

107 The effect of task engagement on auditory cortical neurons can persist for several minutes or
108 hours following task termination (13, 23–25, 30, 49). If OFC mediates the changes observed in
109 auditory cortex, OFC neurons should exhibit similar temporal dynamics. Therefore, we asked
110 whether changes in OFC activity persist into the passive sound exposure session immediately
111 following the task. As shown in Figure 2G, the firing rates of task-enhanced units returned to
112 passive-pre levels after the task was over ($p > 0.999$, see Table 1 for full statistical results). In
113 contrast, task-suppressed units exhibited longer-lasting changes, such that firing rates during the

114 passive-post session remained significantly lower than during the passive-pre session ($p < 0.001$).
115 All findings above were replicated when our analyses were restricted to single-units (Figure S3).

116

117 Together, these data reveal that a subset of OFC neurons exhibit task-dependent modulations
118 that evolve over a similar time course as those observed in the auditory cortex and raise the
119 possibility that task-dependent changes in OFC and the auditory cortex are mechanistically linked.

120 *OFC inactivation impairs AM detection behavior*

121 Task-dependent modulation of the auditory cortex is believed to enhance the detection or
122 discrimination of behaviorally relevant stimuli (13, 17, 18, 20, 22, 23, 27, 28, 42–46, 48). If OFC
123 mediates task-dependent modulations in the auditory cortex, then suppressing OFC activity should
124 impair sound detection. To test this prediction, we implanted cannulas in bilateral OFC of nine
125 gerbils (six females) previously trained to detect AM stimuli. In one male and one female, right
126 hemisphere infusion cannulas clogged, but data from these animals were still included to evaluate
127 the effect of unilateral left OFC inactivation. On alternating days, we infused either saline or
128 muscimol (a GABA_a agonist that reversibly silences neural activity) into the OFC shortly before
129 animals performed the AM detection task (Figure 3A-B).

130

131 OFC inactivation significantly impaired AM detection. As shown in Figure 3C, behavioral d'
132 values were lower (poorer) in all animals tested after muscimol was infused into the OFC, compared
133 to when saline was infused ($p < 0.001$; see Table 1 for full statistical results). Impaired performance
134 could not be explained by reduced motivation to engage in the task, as the amount of water
135 consumed (Figure 3D) and the number of AM trials completed (Figure 3E) were unaffected by
136 muscimol infusion (both $p > 0.1$). However, OFC inactivation did reduce the rate of trial completion
137 ($p = 0.002$, Figure 3F). This observation might be explained by the fact that the poor performance
138 caused by muscimol infusion resulted in animals receiving more frequent punishment, thereby
139 generating more frequent (and longer) spout withdrawals. Indeed, miss rates strongly predicted
140 rates of trial completion ($p < 0.001$; Figure S4A).

141

142 OFC inactivation may have impaired behavioral performance by disrupting an animal's ability
143 to detect the AM sound cue (thereby reducing the hit rate), and/or by increasing indiscriminate
144 responding to the unmodulated noise (thereby increasing the false alarm rate). This latter scenario
145 is important to consider, as OFC lesions have been associated with changes in impulsive behavior
146 (50, 51). To address this issue, we asked how muscimol infusion separately impacted hit rates and
147 false alarm rates. We found that muscimol treatment drastically reduced hit rates in all animals
148 tested ($p < 0.001$; Figure 3G). In contrast, muscimol treatment only marginally increased false alarm
149 rates ($p = 0.039$; Figure 3H). This small uptick in false alarm rates might be explained by the fact
150 that animals that receive more frequent punishment are more hesitant to stay on the spout. Indeed,
151 miss rates strongly predicted false alarm rates ($p = 0.001$; Figure S4B). Collectively, these
152 observations suggest that after OFC inactivation, animals struggled to detect AM noise.

153 *OFC inactivation prevents task-dependent modulation of auditory cortical neurons*

154 Task-dependent modulations of auditory cortical activity are not fixed in magnitude, and their
155 strength correlates with behavioral AM detection abilities. Strong modulations are associated with
156 excellent AM detection skills, whereas small modulations are associated with poor performance
157 (13). This observation, together with the findings presented above, raises the possibility that OFC

158 inactivation impairs behavioral AM detection by disrupting task-dependent modulations of auditory
159 cortical activity.

160

161 To test this hypothesis, we implanted three gerbils (one male) with cannulas in bilateral OFC
162 and a 64-channel silicon probe in left auditory cortex. We initially recorded 22 single- and 45 multi-
163 units in layer 2/3 of the auditory cortex during passive sound exposure. We then infused saline or
164 muscimol into the OFC and recorded from the same auditory cortical units as the animals performed
165 the AM detection task (Figure 4A). Given the relatively small number of single units recorded under
166 each treatment condition (saline: $n = 12$, muscimol: $n = 10$), we pooled single- and multi-units
167 together for our statistical analyses. Electrode tracks were visualized offline and used to reconstruct
168 recording site locations (Figure 4B).

169

170 We first confirmed that OFC inactivation impaired behavioral performance in these animals. As
171 expected from our previous findings, muscimol infusion reduced behavioral d' values ($p < 0.001$;
172 Figure 4C) and hit rates ($p = 0.004$; Figure S5A) in all subjects without significantly affecting false
173 alarm rates or water consumption (all $p > 0.099$; Figure S5B-C). We then asked how OFC
174 inactivation affected auditory cortical activity. Figure 4D illustrates AM-evoked responses from two
175 representative auditory cortical units from the same animal recorded on different days. The
176 responses in the top row were recorded from one unit before and after saline infusion into the OFC.
177 This unit showed a stronger AM-evoked firing rate during the task than during passive sound
178 exposure, consistent with our previously published work (13). In contrast, the responses in the
179 bottom row, which were recorded from a different unit before and after muscimol infusion into the
180 OFC, showed a moderately reduced firing rate following OFC inactivation.

181

182 To determine whether these differences in response gain translated into differences in AM
183 sensitivity, we transformed the firing rates of individual units into a neural discriminability metric
184 (neural d'), using our previously established approach (13, 52). We report absolute neural d' values
185 here because negative d' values can also support enhanced AM detection via decreases in firing
186 relative to baseline. When saline was infused into OFC, absolute neural d' values were significantly
187 higher during task engagement than during passive sound exposure ($p = 0.007$, Figure 4E), as
188 expected from our prior work (13). In contrast, when muscimol was infused into the OFC, absolute
189 neural d' values during task engagement and passive sound exposure were similar ($p = 0.162$).
190 These data demonstrate that suppressing the OFC prevents task-dependent modulations of the
191 auditory cortex.

192

193 The d' value for each neuron depends on its average firing rate and its firing rate variability
194 during non-AM and AM noise (see Supplementary Methods in SI Appendix). To determine which
195 of these factors are impacted by OFC inactivation, we first examined the firing rates of individual
196 neurons and compared these values between passive and task sessions. We found that task
197 engagement did not systematically affect auditory cortical firing rates evoked by either non-AM or
198 AM noise, regardless of drug treatment (all $p > 0.1$; Figure S6A-B). This observation raised the
199 possibility that the differences we observed in neural d' values are due to joint changes in non-AM
200 and AM noise responses that manifest on a unit-by-unit basis (see Supplementary Methods in SI
201 Appendix and (13)). To test this idea, we calculated the difference between non-AM and AM firing
202 rates for each auditory cortical unit (here termed the ΔFR), and then compared ΔFR values
203 between passive and task sessions. We found that ΔFR significantly increased during task

204 engagement when saline was infused into the OFC ($p = 0.004$). In contrast, ΔFR values remained
205 similar between sessions when muscimol was infused ($p = 0.121$; [Figure 4F](#)).

206

207 We then calculated the coefficient of variation (CV) for each unit as an indicator of firing rate
208 variability and compared CV values between passive and task sessions. Task engagement did not
209 significantly affect non-AM- or AM-evoked CV values, regardless of drug treatment (all $p > 0.4$;
210 [Figure S6C-D](#)), nor did it affect the sum of non-AM and AM CV values (all $p > 0.192$; [Figure 4G](#)).
211 Together, these findings suggest that OFC inactivation prevents a task-dependent increase in the
212 separation of AM and non-AM firing rate distributions, and not a task-dependent reduction in firing
213 rate variability.

214

215 In addition to modulating average firing rates, task engagement can also impact sound
216 encoding and perception by enhancing stimulus phase-locking (27, 43). Therefore, we calculated
217 the phase-projected vector strength evoked by AM noise for individual auditory cortical units and
218 compared these values between passive and task sessions (27, 43, 53). We found that task
219 engagement had no effect on vector strength regardless of drug treatment (all $p > 0.625$; [Figure](#)
220 [4H](#)). This finding is consistent with the observation that task-dependent effects on phase-locking
221 are more significant when AM depths are small (27).

222

223 Collectively, these results indicate that OFC inactivation prevents context-dependent
224 enhancements of behaviorally-relevant sound representations in the auditory cortex by modifying
225 neuronal firing rates, without affecting neuronal phase-locking.

226 *Compensatory mechanisms restore behavioral and auditory cortical AM sensitivity after repeated* 227 *OFC inactivation*

228 In two subjects (one female) chronically implanted with OFC cannulas and auditory cortex
229 electrodes, we infused saline or muscimol into the OFC multiple times over several days in an
230 attempt to enlarge our sample of auditory cortical neurons. However, we noticed that the
231 effectiveness of repeated muscimol infusions quickly waned and ultimately failed to significantly
232 impact behavior ([Figure 5A](#)), indicative of a compensatory mechanism after whole-session OFC
233 inactivation (54, 55).

234

235 We took advantage of this variability to ask whether muscimol's effectiveness, inferred from
236 downstream auditory cortical AM sensitivity, predicted behavioral AM detection. We recorded from
237 60 single- and 96 multi-units over ten days. Indeed, behavioral d' significantly correlated with neural
238 d' during the task ($p = 0.002$; [Figure 5B](#)). To highlight this relationship, we compared neural d'
239 values from the two worst performance days from each animal with the two best days (regardless
240 of drug treatment). We found that neural d' values were significantly higher when behavioral
241 performance was good than when performance was poor ($p < 0.001$; [Figure 5C](#)). These findings
242 suggest that OFC is a key part of a distributed network that provides contextual information to the
243 auditory cortex, and when OFC activity is repeatedly suppressed, other brain regions may be
244 recruited to compensate for the loss.

245 **Discussion**

246 Context-dependent modulation is a widely reported feature of the auditory cortex and is
247 hypothesized to adaptively modify the perceptual salience of stimuli in response to moment-to-

248 moment changes in their behavioral relevance (13, 17, 18, 20, 22, 23, 27, 28, 42–46, 48). Although
249 prior work has identified several brain regions capable of modifying auditory cortical responses and
250 behavior (40, 48, 56–58), our understanding of the neural networks that mediate rapid shifts in
251 auditory perception remains limited. In this study, we reveal that a subset of OFC neurons are
252 sensitive to behavioral context, exhibiting task-dependent dynamics that mirror those previously
253 observed in the auditory cortex (13, 23–25, 30, 49). Our pharmacological experiments demonstrate
254 that OFC inactivation prevents task-dependent enhancements of auditory cortical sensitivity, and,
255 in turn, impairs the ability of animals to detect AM noise. Notably, the behavioral effect of repeated
256 whole-session OFC inactivation gradually waned, suggesting that compensatory brain regions may
257 be recruited when OFC output is unavailable. Together, our results suggest that OFC provides
258 contextual information to the auditory cortex to facilitate the perception of behaviorally relevant
259 sounds.

260

261 We found that the OFC is strongly modulated by behavioral context. Both the OFC neuronal
262 population as a whole and the specific subset of neurons that innervate the auditory cortex
263 represent behaviorally relevant cues, such as trial outcome, when gerbils perform a sound
264 detection task. These results are consistent with a recent report from mice (41) and support the
265 idea that the OFC makes an important contribution to auditory cortical sound processing and
266 perception.

267

268 During both passive sound exposure and task engagement, OFC neurons were largely
269 unresponsive to AM stimuli. This finding differs from prior work documenting sound-evoked activity
270 in OFC neurons across behavioral states and even under anesthesia (41, 59–61). One possible
271 explanation for this apparent discrepancy is the fact that OFC neurons exhibit relatively poor
272 broadband noise thresholds (e.g. \geq ~50 dB SPL) (60, 61), and all prior studies characterized OFC
273 sound responses at or well above this intensity. Our stimuli, in contrast, were presented at 45 dB
274 SPL and were therefore likely below threshold for most or all OFC neurons. Intriguingly, despite
275 the fact that our acoustic stimuli did not systematically evoke OFC activity, we still observed
276 profound effects of OFC inactivation on auditory cortical plasticity and behavioral output. These
277 results suggest that auditory cortical inputs to the OFC may not be necessary for OFC to
278 successfully signal contextual information back to the auditory cortex. Future experiments could
279 test this hypothesis by silencing auditory cortical axon terminals in the OFC during sound-guided
280 behavior.

281

282 We found that OFC inactivation reduces the sensitivity of auditory cortical neurons to behavioral
283 context and impairs behavioral performance of an AM detection task. These data suggest that OFC
284 plays a key role in transmitting contextual information to the auditory cortex to shape sound
285 perception, but the route(s) by which such information is transmitted remains uncertain. Several
286 recent studies support the involvement of a monosynaptic pathway. For example, OFC axon
287 terminals in mouse auditory cortex are sensitive to listening conditions and encode behavioral
288 choice (41). Optogenetic stimulation of these terminals reshapes auditory cortical frequency tuning
289 in anesthetized mice (59), and silencing of these terminals disrupts the ability of animals to flexibly
290 categorize sounds (40). Similar OFC terminal manipulations in the visual or somatosensory cortices
291 alter sensory-evoked responses and impact sensory learning (38, 39). These data suggest that
292 direct projections from the OFC convey contextual information to sensory cortices to modulate
293 stimulus perception.

294

295 OFC may also support context-dependent plasticity in sensory cortices via multi-synaptic
296 pathways that recruit neuromodulatory centers. For instance, cholinergic input from the nucleus
297 basalis alters auditory cortical receptive fields and sound perception, and cholinergic axons
298 increase their activity during sound-guided behavior (48, 62–66). Similarly, dopaminergic input from
299 the ventral tegmental area (VTA) influences thalamocortical gain and receptive field organization
300 in the auditory cortex, and is implicated in auditory avoidance learning (67–70). OFC projects to
301 both nucleus basalis (32, 71) and the VTA (72) and regulates VTA firing (73). Thus, OFC neurons
302 may indirectly shape auditory cortical processing and sound perception by relaying contextual
303 information to cholinergic or dopaminergic neurons that innervate the auditory cortex. Targeted
304 manipulations of OFC axons in the nucleus basalis and VTA are needed to resolve these
305 possibilities.

306
307 We previously found that task-dependent modulations of auditory cortical neurons grow
308 stronger as animals learn to detect small, near-threshold amplitude modulations (13). This
309 observation suggests that the non-sensory inputs that rapidly modulate auditory cortical activity
310 during task performance also mediate the gradual, longer-term plasticity processes that underlie
311 perceptual learning. This idea is supported by human behavioral experiments demonstrating that
312 in some cases, perceptual learning can be generated by interleaving brief bouts of practice (which
313 are too short to drive learning on their own) with passive sound exposure (74). These data suggest
314 that (I) the non-sensory processes engaged by task performance remain active for some time after
315 task performance ends, and (II) if sounds are passively presented during these periods of residual
316 non-sensory activity, learning can occur. This interpretation closely matches our neurophysiological
317 findings: both auditory cortical (13) and a subset of OFC neurons exhibit task-dependent changes
318 in activity that persist for several minutes after the task has ended. Taken together, these findings
319 support a conceptual framework that task engagement puts sensory cortical neurons into a
320 'sensitized' state permissive for learning, which lasts for many minutes beyond the end of the task
321 (13, 23, 75, 76). The neural circuits involved in regulating this phenomenon are still unclear, but
322 our data suggest that a subpopulation of OFC neurons may be involved. Future work should use
323 viral approaches to identify the downstream targets of these neurons, and to determine their causal
324 contributions to task-induced sensitization of sensory circuits and practice-based improvements in
325 auditory perception.

326 **Materials and Methods**

327 For a full description of the methodology, see Supplementary Materials in the SI Appendix.

328 *Subjects*

329 Adult Mongolian gerbils (*Meriones unguiculatus*) used in this study were bred in-house from
330 commercially obtained breeding pairs (Charles River). Animals were kept under 12 hr light:12 hr
331 dark cycle and on *ad libitum* food, enrichment and water access until placed on controlled water
332 access for behavioral experiments. All procedures were approved by the Institutional Animal Care
333 and Use Committee at the University of Maryland College Park.

334 *Behavioral task and passive sound exposure*

335 Auditory perception was tested with an aversive go/no-go amplitude-modulated (AM) detection
336 task as previously described (13, 52, 77–80). Briefly, unmodulated broadband noise was

337 continuously presented from a calibrated speaker and unpredictably transitioned into AM noise
338 while animals drank from a water spout. AM detection performance was assessed by $d' = z(HR) -$
339 $z(FAR)$, where $z(HR)$ and $z(FAR)$ are the z-scores at the probability levels of hit rates (HR) and
340 false alarm rates (FAR). For passive sound exposure, the waterspout was removed from arena,
341 and unmodulated noise transitioned to AM noise pseudorandomly every 3-5 s.

342 *Electrophysiology*

343 Extracellular neural activity was recorded chronically from either left OFC or left auditory cortex.
344 After spike sorting, auditory cortical firing rates were transformed to neural d' (13, 46). The ability
345 of the units to phase-lock to the 5 Hz AM stimulus was analyzed by calculating the phase-projected
346 vector strength (53). The backs of electrode shanks were painted with azide-free fluorescent
347 microspheres (FluoSpheres 0.2 μm ; ThermoFisher) before implantation to verify implant site
348 location *post mortem*.

349 *Software and analysis*

350 Statistical analyses were performed using R (version 4.3.1) and RStudio (version 2023.9.1.494;
351 Posit Software). All statistical results can be found in Table 1. Boxplots center lines represent
352 medians, boxes represent 25-75% interquartile range and whiskers represent 10-90% interquartile
353 ranges.

354 *Brain infusions*

355 Muscimol (1-2 $\mu\text{g}/\mu\text{L}$; 0.25-0.5 $\mu\text{L}/\text{hemisphere}$) or vehicle (0.9% saline) was infused through
356 chronic bilateral cannula targeting OFC ~40 min before the task.

357 **Acknowledgments**

358 We thank current and former members of the Caras Lab for helpful feedback and discussions
359 and assistance with animal care. Special thanks to Dr. Daniel Stolzberg for assistance with software
360 for behavioral testing. We acknowledge the Imaging Core Facility in the department of Cell Biology
361 and Molecular Genetics at the University of Maryland, College Park for training and the use of the
362 Zeiss LSM 980 Airyscan 2 confocal microscope. Purchase of the Zeiss LSM 980 Airyscan 2 was
363 supported by Award Number 1S10OD025223-01A1 from the National Institute of Health (NIH). This
364 work was supported by NIH R00DC016046 and R01DC020742 to MLC.

References

1. E. Asutay, D. Västfjäll, Perception of Loudness Is Influenced by Emotion. *PLoS ONE* **7**, e38660 (2012).
2. D. Kim, S. Lokey, S. Ling, Elevated arousal levels enhance contrast perception. *Journal of Vision* **17**, 1–10 (2017).
3. M. Mather, M. R. Sutherland, Arousal-Biased Competition in Perception and Memory. *Perspect Psychol Sci* **6**, 114–133 (2011).
4. M. J. McGinley, S. V. David, D. A. McCormick, Cortical Membrane Potential Signature of Optimal States for Sensory Signal Detection. *Neuron* **87**, 179–192 (2015).
5. B. G. Shinn-Cunningham, Object-based auditory and visual attention. *Trends in Cognitive Sciences* **12**, 182–186 (2008).
6. H. Spitzer, R. Desimone, J. Moran, Increased Attention Enhances Both Behavioral and Neuronal Performance. *Science* **240**, 338–340 (1988).
7. R. H. Ashton, “Nothing Good Ever Came from New Jersey”: Expectations and the Sensory Perception of Wines. *J Wine Econ* **9**, 304–319 (2014).
8. A. I. Carcea, M. N. Insanally, R. C. Froemke, Dynamics of cortical activity during behavioral engagement and auditory perception. *Nature Communications* **8**, 1–12 (2017).
9. F. P. De Lange, M. Heilbron, P. Kok, How Do Expectations Shape Perception? *Trends in Cognitive Sciences* **22**, 764–779 (2018).
10. Y. Pinto, S. Van Gaal, F. P. De Lange, V. A. F. Lamme, A. K. Seth, Expectations accelerate entry of visual stimuli into awareness. *Journal of Vision* **15**, 1–15 (2015).
11. T. Stein, M. V. Peelen, Content-specific expectations enhance stimulus detectability by increasing perceptual sensitivity. *Journal of Experimental Psychology: General* **144**, 1089–1104 (2015).
12. S. Vangkilde, J. T. Coull, C. Bundesen, Great expectations: Temporal expectation modulates perceptual processing speed. *Journal of Experimental Psychology: Human Perception and Performance* **38**, 1183–1191 (2012).
13. M. L. Caras, D. H. Sanes, Top-down modulation of sensory cortex gates perceptual learning. *Proceedings of the National Academy of Sciences of the United States of America* **114**, 9972–9977 (2017).
14. C. E. Chapman, E.-M. Meftah, Independent Controls of Attentional Influences in Primary and Secondary Somatosensory Cortex. *Journal of Neurophysiology* **94**, 4094–4107 (2005).
15. M. R. Cohen, J. H. R. Maunsell, Attention improves performance primarily by reducing interneuronal correlations. *Nat Neurosci* **12**, 1594–1600 (2009).
16. S. V. David, J. B. Fritz, S. A. Shamma, Task reward structure shapes rapid receptive field plasticity in auditory cortex. *Proceedings of the National Academy of Sciences of the United States of America* **109**, 2144–2149 (2012).
17. H. Davis, Enhancement of Evoked Cortical Potentials in Humans Related to a Task Requiring a Decision. *Science* **145**, 182–183 (1964).
18. G. De Franceschi, T. R. Barkat, Task-induced modulations of neuronal activity along the auditory pathway. *Cell Reports* **37**, 110115 (2021).
19. J. D. Downer, B. Rapone, J. Verhein, K. N. O'Connor, M. L. Sutter, Feature-Selective Attention Adaptively Shifts Noise Correlations in Primary Auditory Cortex. *J. Neurosci.* **37**, 5378–5392 (2017).
20. J. D. Downer, M. Niwa, M. L. Sutter, Task engagement selectively modulates neural correlations in primary auditory cortex. *Journal of Neuroscience* **35**, 7565–7574 (2015).

21. A. Fontanini, D. B. Katz, State-Dependent Modulation of Time-Varying Gustatory Responses. *Journal of Neurophysiology* **96**, 3183–3193 (2006).
22. N. A. Francis, *et al.*, Small Networks Encode Decision-Making in Primary Auditory Cortex. *Neuron* **97**, 885–897.e6 (2018).
23. J. Fritz, S. Shamma, M. Elhilali, D. Klein, Rapid task-related plasticity of spectrotemporal receptive fields in primary auditory cortex. *Nature Neuroscience* **6**, 1216–1223 (2003).
24. J. B. Fritz, M. Elhilali, S. V. David, S. A. Shamma, Auditory attention - focusing the searchlight on sound. *Current Opinion in Neurobiology* **17**, 437–455 (2007).
25. J. B. Fritz, M. Elhilali, S. A. Shamma, Differential Dynamic Plasticity of A1 Receptive Fields during Multiple Spectral Tasks. *J. Neurosci.* **25**, 7623–7635 (2005).
26. D. H. Hubel, C. O. Henson, A. Rupert, R. Galambos, “Attention” Units in the Auditory Cortex. *Science* **129**, 1279–1280 (1959).
27. M. Niwa, J. S. Johnson, K. N. O’Connor, M. L. Sutter, Active engagement improves primary auditory cortical neurons’ ability to discriminate temporal modulation. *Journal of Neuroscience* **32**, 9323–9334 (2012).
28. A. Sheikhattar, *et al.*, Extracting neuronal functional network dynamics via adaptive Granger causality analysis. *Proc. Natl. Acad. Sci. U.S.A.* **115** (2018).
29. P. N. Steinmetz, *et al.*, Attention modulates synchronized neuronal firing in primate somatosensory cortex. **404** (2000).
30. P. Yin, J. B. Fritz, S. A. Shamma, Rapid Spectrotemporal Plasticity in Primary Auditory Cortex during Behavior. *J. Neurosci.* **34**, 4396–4408 (2014).
31. T. Yoshida, D. B. Katz, Control of Prestimulus Activity Related to Improved Sensory Coding within a Discrimination Task. *J. Neurosci.* **31**, 4101–4112 (2011).
32. L. Gao, *et al.*, Single-neuron projectome of mouse prefrontal cortex. *Nat Neurosci* **25**, 515–529 (2022).
33. H. B. M. Uylings, C. G. Van Eden, “Chapter 3 Qualitative and quantitative comparison of the prefrontal cortex in rat and in primates, including humans” in *Progress in Brain Research*, (Elsevier, 1991), pp. 31–62.
34. P. Enel, A. Q. Perkins, E. L. Rich, Heterogeneous value coding in orbitofrontal populations. *Behavioral Neuroscience* **135**, 245–254 (2021).
35. J. C. B. Azzi, A. Sirigu, J.-R. Duhamel, Modulation of value representation by social context in the primate orbitofrontal cortex. *Proc. Natl. Acad. Sci. U.S.A.* **109**, 2126–2131 (2012).
36. A. Farovik, *et al.*, Orbitofrontal Cortex Encodes Memories within Value-Based Schemas and Represents Contexts That Guide Memory Retrieval. *J. Neurosci.* **35**, 8333–8344 (2015).
37. A. M. Wikenheiser, M. P. H. Gardner, L. E. Mueller, G. Schoenbaum, Spatial representations in rat orbitofrontal cortex. *Journal of Neuroscience* (2021) <https://doi.org/10.1523/JNEUROSCI.0830-21.2021>.
38. A. Banerjee, *et al.*, Value-guided remapping of sensory circuits by lateral orbitofrontal cortex in reversal learning. *Nature* **585** (2020).
39. D. Liu, *et al.*, Orbitofrontal control of visual cortex gain promotes visual associative learning. *Nature Communications* **11**, 1–14 (2020).
40. Y. Liu, Y. Xin, N.-L. Xu, A cortical circuit mechanism for structural knowledge-based flexible sensorimotor decision-making. *Neuron*, 1–16 (2021).
41. J. K. Mittelstadt, P. O. Kanold, Orbitofrontal cortex conveys stimulus and task information to the auditory cortex. *Current Biology* **33**, 4160–4173.e4 (2023).
42. T. E. Mast, C. S. Watson, Attention and auditory evoked responses to low-detectability signals. *Perception & Psychophysics* **4**, 237–240 (1968).

43. M. Niwa, K. N. O'Connor, E. Engall, J. S. Johnson, M. L. Sutter, Hierarchical effects of task engagement on amplitude modulation encoding in auditory cortex. *Journal of Neurophysiology* **113**, 307–327 (2015).
44. B. E. Pfungst, T. A. O'Connor, J. M. Miller, Response plasticity of neurons in auditory cortex of the rhesus monkey. *Exp Brain Res* **29–29** (1977).
45. D. Saderi, Z. P. Schwartz, C. R. Heller, J. R. Pennington, S. V. David, Dissociation of task engagement and arousal effects in auditory cortex and midbrain. *eLife* **10**, 21–25 (2021).
46. G. von Trapp, B. N. Buran, K. Sen, M. N. Semple, D. H. Sanes, A decline in response variability improves neural signal detection during auditory task performance. *Journal of Neuroscience* **36**, 11097–11106 (2016).
47. P. H. Rudebeck, E. A. Murray, The Orbitofrontal Oracle: Cortical Mechanisms for the Prediction and Evaluation of Specific Behavioral Outcomes. *Neuron* **84**, 1143–1156 (2014).
48. K. V. Kuchibhotla, *et al.*, Parallel processing by cortical inhibition enables context-dependent behavior. *Nature Neuroscience* **20**, 62–71 (2017).
49. S. Atiani, M. Elhilali, S. V. David, J. B. Fritz, S. A. Shamma, Task Difficulty and Performance Induce Diverse Adaptive Patterns in Gain and Shape of Primary Auditory Cortical Receptive Fields. *Neuron* **61**, 467–480 (2009).
50. M. M. Torregrossa, J. J. Quinn, J. R. Taylor, Impulsivity, Compulsivity, and Habit: The Role of Orbitofrontal Cortex Revisited. *Biological Psychiatry* **63**, 253–255 (2008).
51. C. A. Winstanley, D. E. H. Theobald, R. N. Cardinal, T. W. Robbins, Contrasting Roles of Basolateral Amygdala and Orbitofrontal Cortex in Impulsive Choice. *J. Neurosci.* **24**, 4718–4722 (2004).
52. M. L. Caras, D. H. Sanes, Neural variability limits adolescent skill learning. *Journal of Neuroscience* **39**, 2889–2902 (2019).
53. P. Yin, J. S. Johnson, K. N. O'Connor, M. L. Sutter, Coding of Amplitude Modulation in Primary Auditory Cortex. *Journal of Neurophysiology* **105**, 582–600 (2011).
54. C. Cazares, D. C. Schreiner, M. L. Valencia, C. M. Gremel, Orbitofrontal cortex populations are differentially recruited to support actions. *Current Biology* **32**, 4675-4687.E5 (2022).
55. H. C. Lasseter, D. R. Ramirez, X. Xie, R. A. Fuchs, Involvement of the lateral orbitofrontal cortex in drug context-induced reinstatement of cocaine-seeking behavior in rats: Orbitofrontal cortex and cocaine seeking. *European Journal of Neuroscience* **30**, 1370–1381 (2009).
56. E. Glennon, *et al.*, Locus coeruleus activation accelerates perceptual learning. *Brain Research* **1709**, 39–49 (2019).
57. B. J. Marlin, *et al.*, Oxytocin enables maternal behaviour by balancing cortical inhibition. *Nature* **520**, 499–504 (2015).
58. A. Schroeder, *et al.*, Inhibitory top-down projections from zona incerta mediate neocortical memory. *Neuron* **111**, 727-738.e8 (2023).
59. D. E. Winkowski, *et al.*, Orbitofrontal Cortex Neurons Respond to Sound and Activate Primary Auditory Cortex Neurons. *Cerebral cortex* **28**, 868–879 (2018).
60. S. Sharma, S. Bandyopadhyay, Differential Rapid Plasticity in Auditory and Visual Responses in the Primarily Multisensory Orbitofrontal Cortex. *eNeuro* **7**, 1–17 (2020).
61. H. Srivastava, S. Bandyopadhyay, Parallel lemniscal and non-lemniscal sources control auditory responses in the orbitofrontal cortex (OFC). *eNeuro* **7**, 1–19 (2020).
62. R. C. Froemke, *et al.*, Long-term modification of cortical synapses improves sensory perception. *Nat Neurosci* **16**, 79–88 (2013).

63. R. C. Froemke, M. M. Merzenich, C. E. Schreiner, A synaptic memory trace for cortical receptive field plasticity. *Nature* **450**, 425–429 (2007).
64. W. Guo, B. Robert, D. B. Polley, The Cholinergic Basal Forebrain Links Auditory Stimuli with Delayed Reinforcement to Support Learning. *Neuron* **103**, 1164–1177.e6 (2019).
65. A. A. Miasnikov, J. C. Chen, N. M. Weinberger, Rapid induction of specific associative behavioral memory by stimulation of the nucleus basalis in the rat. *Neurobiology of Learning and Memory* **86**, 47–65 (2006).
66. A. A. Miasnikov, J. C. Chen, N. M. Weinberger, Specific auditory memory induced by nucleus basalis stimulation depends on intrinsic acetylcholine. *Neurobiology of Learning and Memory* **90**, 443–454 (2008).
67. S. Bao, V. T. Chan, M. M. Merzenich, Cortical remodelling induced by activity of ventral tegmental dopamine neurons. *Nature* **412**, 79–83 (2001).
68. M. G. K. Brunk, *et al.*, Optogenetic stimulation of the VTA modulates a frequency-specific gain of thalamocortical inputs in infragranular layers of the auditory cortex. *Scientific Reports* **9**, 1–15 (2019).
69. M. F. K. Happel, M. Deliano, J. Handschuh, F. W. Ohl, Dopamine-Modulated Recurrent Corticoefferent Feedback in Primary Sensory Cortex Promotes Detection of Behaviorally Relevant Stimuli. *Journal of Neuroscience* **34**, 1234–1247 (2014).
70. H. Stark, H. Scheich, Dopaminergic and serotonergic neurotransmission systems are differentially involved in auditory cortex learning: a long-term microdialysis study of metabolites. *Journal of neurochemistry* **68**, 691–7 (1997).
71. F. T. Russchen, D. G. Amaral, J. L. Price, The afferent connections of the substantia innominata in the monkey, *Macaca fascicularis*. *J. Comp. Neurol.* **242**, 1–27 (1985).
72. M. Watabe-Uchida, L. Zhu, S. K. Ogawa, A. Vamanrao, N. Uchida, Whole-Brain Mapping of Direct Inputs to Midbrain Dopamine Neurons. *Neuron* **74**, 858–873 (2012).
73. Y. S. Jo, S. J. Y. Mizumori, Prefrontal Regulation of Neuronal Activity in the Ventral Tegmental Area. *Cereb. Cortex* **26**, 4057–4068 (2016).
74. D. F. Little, H. H. Cheng, B. A. Wright, Inducing musical-interval learning by combining task practice with periods of stimulus exposure alone. *Attention, Perception, & Psychophysics* **81**, 344–357 (2018).
75. A. R. Seitz, H. R. Dinse, A common framework for perceptual learning. *Current Opinion in Neurobiology* **17**, 148–153 (2007).
76. B. A. Wright, A. T. Sabin, Y. Zhang, N. Marrone, M. B. Fitzgerald, Enhancing perceptual learning by combining practice with periods of additional sensory stimulation. *Journal of Neuroscience* **30**, 12868–12877 (2010).
77. M. L. Caras, D. H. Sanes, Sustained perceptual deficits from transient sensory deprivation. *Journal of Neuroscience* **35**, 10831–10842 (2015).
78. E. C. Sarro, G. Von Trapp, T. M. Mowery, V. C. Kotak, D. H. Sanes, Cortical Synaptic Inhibition Declines during Auditory Learning. *J. Neurosci.* **35**, 6318–6325 (2015).
79. E. C. Sarro, D. H. Sanes, Prolonged maturation of auditory perception and learning in gerbils. *Devel Neurobio* **70**, 636–648 (2010).
80. E. C. Sarro, D. H. Sanes, The Cost and Benefit of Juvenile Training on Adult Perceptual Skill. *J. Neurosci.* **31**, 5383–5391 (2011).

Figures and Tables

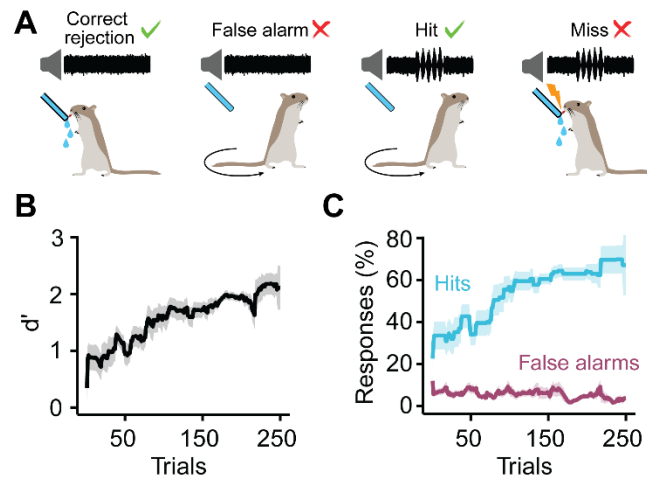


Figure 1. Behavioral task. (A) Task structure. Water-deprived animals were trained to drink from a waterspout while unmodulated noise continuously played from a speaker, and to withdraw from the spout upon presentation of amplitude-modulated (AM) noise. Failing to withdraw during AM noise was punished with a mild shock. (B-C) Mean \pm standard error d' values (B) or hit rates and false alarm rates (C) for all animals included in this study ($n = 16$). Data were concatenated from training sessions over six days and analyzed using a 20-trial sliding window. Animals were only used for experiments after they reached expert performance levels ($d' \geq 2$).

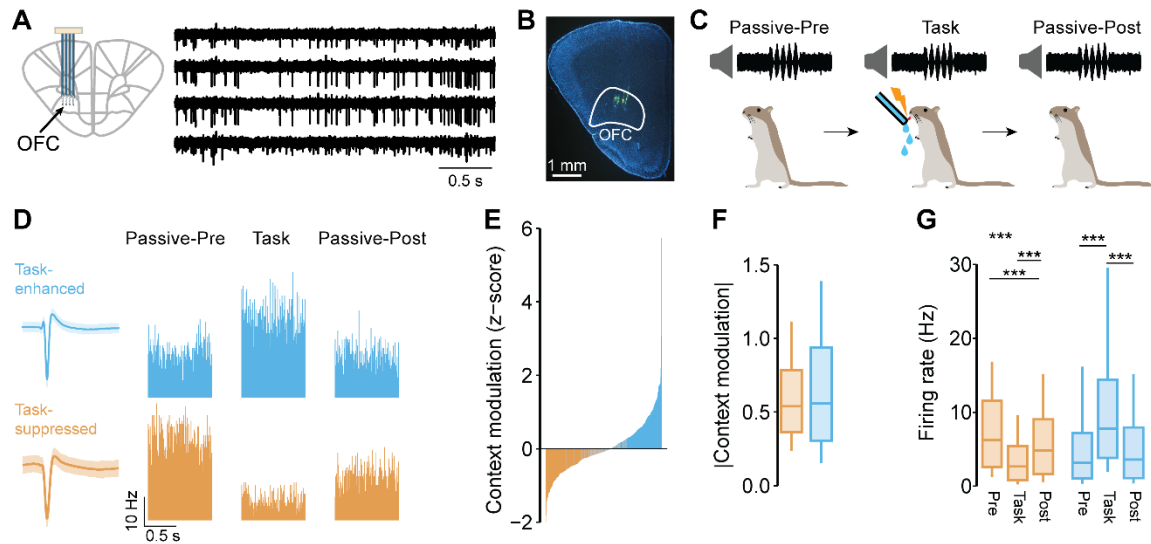


Figure 2. OFC neurons are sensitive to behavioral context. (A) Extracellular recordings were made from 64-channel electrode arrays chronically inserted into the left OFC. Sample recordings illustrate filtered voltage traces from four adjacent channels capturing activity from the same unit. (B) Histological images were used to confirm electrode placement by visualizing fluorescently labeled tracks (green) in the OFC. (C) OFC activity was recorded during task engagement and during passive sound exposure sessions just before ('passive-pre') and just after ('passive-post') the task. The same units were recorded across all three sessions. (D) Peristimulus time-histograms of two representative OFC neurons illustrate the effect of task engagement on non-AM firing rates. The 'task-enhanced' neuron (blue) exhibited a significant increase in firing during the task, while the 'task-suppressed' neuron (orange) exhibited a significant decrease. Mean \pm standard deviation waveforms for each unit are shown on the left. (E) The magnitude of context modulation for each unit was calculated as the difference between the non-AM firing rate during the task and the non-AM firing rate during the passive-pre session z-scored over trials. Modulation values are presented for all units sorted in increasing order. Gray bars represent units without significant contextual modulation. (F) Absolute modulation magnitudes were similar between task-enhanced and -suppressed units. (G) Task-suppressed units exhibited reductions in non-AM firing that persisted into the passive-post period. The activity of task-enhanced units, on the other hand, returned to passive-pre levels after the task ended. *** $p < 0.001$

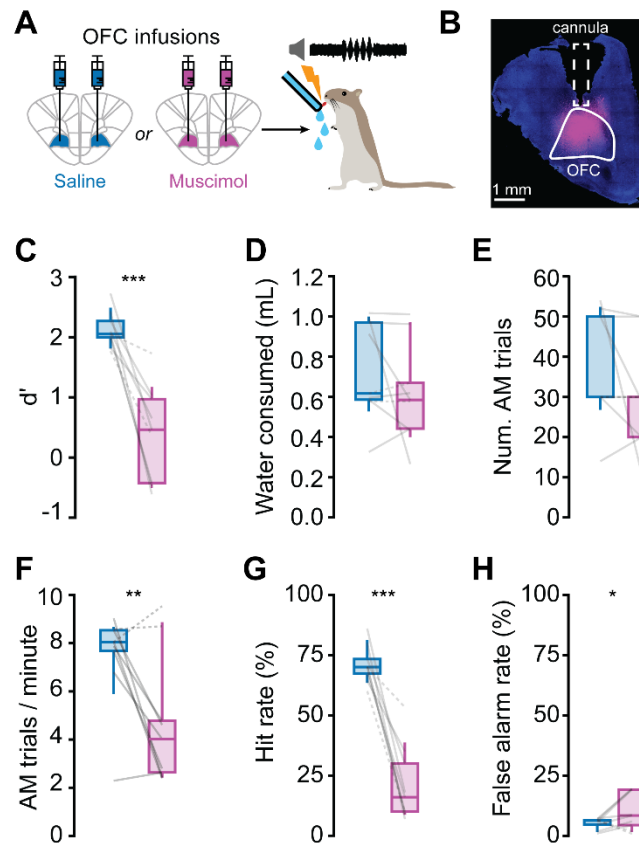


Figure 3. OFC inactivation impairs behavioral AM detection. (A) On alternating days, muscimol or saline was infused into bilateral OFC ~40 minutes before animals performed the AM detection task. (B) At the conclusion of the experiment, a fluororuby infusion just prior to transcardial perfusion provided an estimation of drug spread. (C-E) Muscimol infusions reduced behavioral d' values (C), without systematically affecting water consumption (D) or the number of completed AM trials (E). However, muscimol infusion did reduce the rate of AM trial completion (F). (G-H) Muscimol infusions significantly reduced hit rates (G), and only slightly increased false alarm rates (H). Dashed lines indicate data from animals that received unilateral left infusions due to partially clogged cannulas. * $p < 0.05$, ** $p < 0.01$, *** $p < 0.001$.

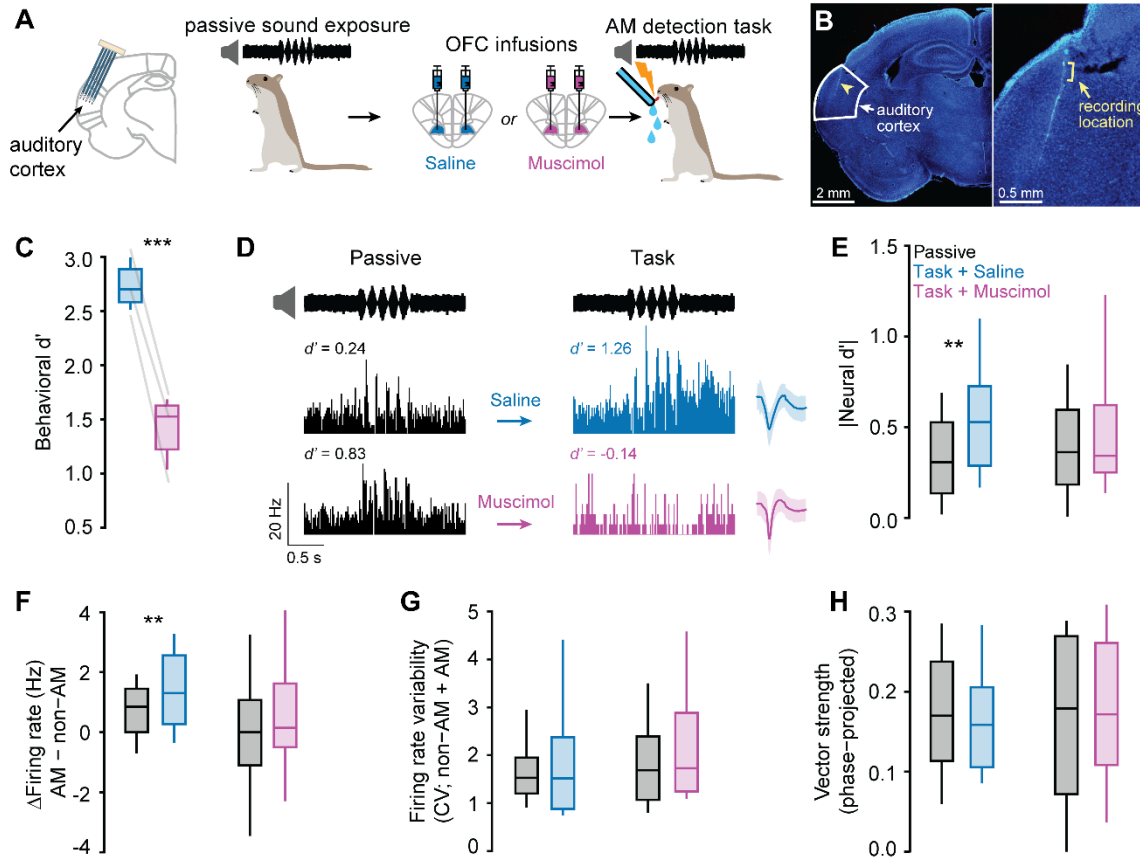


Figure 4. OFC inactivation prevents contextual modulation of auditory cortical neurons. (A) Auditory cortical multi- and single-units were chronically recorded while animals were passively exposed to sounds. Animals then received muscimol or saline infusions in bilateral OFC. Following the infusions, recordings were again made from the same auditory cortical units while animals performed the AM detection task. (B) Electrode placement was confirmed to be in auditory cortex by visualizing fluorescently labeled tracks (green) post-mortem. Recording sites were estimated to be in layers 2/3 (brackets in inset). (C) OFC inactivation impaired behavioral AM detection, replicating the results presented in Figure 3. (D) AM-evoked responses are shown from two representative auditory cortical units recorded from the same animal on different days. Top: An auditory cortical unit recorded before and after saline infusion into the OFC exhibits stronger AM-evoked firing during the task than during passive sound exposure, consistent with our previously published work (13). Bottom: An auditory cortical unit recorded before and after muscimol infusion into the OFC exhibits a modestly reduced firing rate during the task compared to passive sound exposure. (E-F) OFC inactivation prevents a task-dependent increase in auditory cortical neural d' values (E) and prevents a task-dependent increase in the separation of AM and non-AM firing rate distributions (F). This separation (termed Δ Firing Rate) was calculated for each unit as the difference between AM-evoked and non-AM-evoked firing rates. (G-H) Neither task engagement nor OFC inactivation affected firing rate variability (G) or phase-locking (H). $**p < 0.01$, $***p < 0.001$.

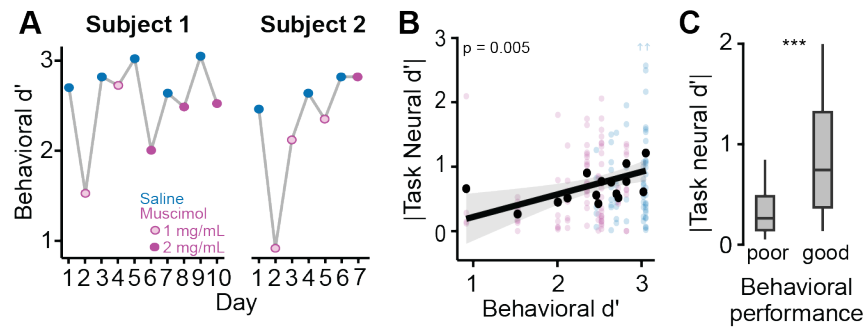


Figure 5. Auditory cortical AM sensitivity correlates with behavioral performance. (A) Repeated muscimol injections into bilateral OFC exert progressively weaker effects on behavior in two subjects. Doubling the muscimol concentration (dark magenta) modestly restored the behavioral effect in one subject (left). (B) Absolute neural d' values for individual auditory cortical units (small translucent points) are plotted as a function of the behavioral d' value obtained during the recording session. Black points illustrate median absolute neural d' for each behavioral d' value. Blue arrows indicate two points that exceeded the depicted range of neural d' values. Neural and behavioral d' values are significantly correlated (see Table 1 for full statistics). (C) Absolute neural d' values obtained during the task were significantly higher on days when behavioral performance was good (two best days from each animal) versus days when behavioral performance was poor (two worst days from each animal). $n = 30$ units on poor performance days and $n = 49$ units on good performance days. *** $p < 0.001$.

Table 1. Statistical results

Figure	Test	Factor(s)	Statistic	P value
2F	GLM/ANOVA	Type	$\chi^2_1 = 0.207$	0.649
2G	GLM/ANOVA: Task-suppressed Bonferroni: Task-suppressed	Context	$\chi^2_2 = 325.690$	< 0.001
		Pre – Task	$t_{584} = 17.976$	< 0.001
		Pre – Post	$t_{584} = 7.608$	< 0.001
		Task – Post	$t_{584} = -10.368$	< 0.001
	GLM/ANOVA: Task-enhanced Bonferroni: Task-enhanced	Context	$\chi^2_2 = 308.390$	< 0.001
		Pre – Task	$t_{593} = -11.422$	< 0.001
		Pre – Post	$t_{593} = -0.802$	>0.999
		Task – Post	$t_{593} = 11.123$	< 0.001
3C	GLM/ANOVA	Treatment	$\chi^2_1 = 41.851$	< 0.001
3D	GLM/ANOVA	Treatment	$\chi^2_1 = 1.895$	0.169
3E	GLM/ANOVA	Treatment	$\chi^2_1 = 2.599$	0.107
3F	GLM/ANOVA	Treatment	$\chi^2_1 = 9.578$	0.002
3G	GLM/ANOVA	Treatment	$\chi^2_1 = 84.366$	< 0.001
3H	GLM/ANOVA	Treatment	$\chi^2_1 = 4.247$	0.039
4C	GLM/ANOVA	Treatment	$\chi^2_1 = 238.960$	< 0.001
4E	GLM/ANOVA: Saline	Context	$\chi^2_1 = 7.293$	0.007
	GLM/ANOVA: Muscimol	Context	$\chi^2_1 = 1.952$	0.162
4F	GLM/ANOVA: Saline	Context	$\chi^2_1 = 8.280$	0.004
	GLM/ANOVA: Muscimol	Context	$\chi^2_1 = 2.405$	0.121
4G	GLM/ANOVA: Saline	Context	$\chi^2_1 = 0.313$	0.576
	GLM/ANOVA: Muscimol	Context	$\chi^2_1 = 1.706$	0.192
4H	GLM/ANOVA: Saline	Context	$\chi^2_1 < 0.001$	0.978
	GLM/ANOVA: Muscimol	Context	$\chi^2_1 = 0.239$	0.625
5B	GLM/ANOVA	Task behavioral d'	$\chi^2_1 = 7.957$	0.005
5C	GLM/ANOVA	Behavioral performance	$\chi^2_1 = 11.526$	<0.001

Supporting Information for Orbitofrontal Cortex Modulates Auditory Cortical Sensitivity and Sound Perception

Matheus Macedo-Lima, Lashaka Sierra Hamlette, Melissa L. Caras
Department of Biology, University of Maryland, College Park

*Melissa L. Caras

Email: mcaras@umd.edu

This PDF file includes:

- Supporting Information Text
- Figures S1 to S6
- Table S1
- SI References

1 **Supporting Information Text**

2 **Supplementary Methods**

3 *Behavioral set-up*

4 Auditory perception was tested with an aversive go/no-go AM detection task as previously described
5 (1–4). A custom test cage (CCMI Plastics) containing a stainless-steel water spout and metal floor plate
6 was positioned inside a sound attenuating booth (GretchKen). Infrared detection of the animal at the
7 spout triggered water delivery via a programmable syringe pump (NE-1000, New Era Pump Systems).
8 Sound stimuli were delivered via a calibrated free-field speaker (DX25TG59-04 1" Fabric Dome Tweeter,
9 Peerless by Tympany) positioned directly above the test cage. Shocks were delivered by an H13-15
10 Precision Animal Shocker (Colburn). Behavior was monitored remotely via webcam. Data acquisition,
11 sound delivery, and digital outputs were controlled via an RZ6 multifunction processor (Tucker Davis
12 Technologies, TDT).

13

14 *Behavioral training and testing*

15 During an initial procedural training stage, animals were placed on controlled water access and
16 learned to drink steadily from a spout while in the presence of a “safe cue” (unmodulated broadband
17 noise, 0.1-20 kHz, 45 dB SPL). Animals were then trained to withdraw from the spout when the sound
18 changed to the “warn” cue (5 Hz sinusoidal amplitude modulated (AM) noise, 0 dB re: 100% depth, 1
19 second duration) by pairing the warn cue with a mild shock (0.5-1 mA, 300 msec). Warn trials were
20 randomly interspersed with 3-5 safe trials, but only while animals made contact with the spout. The gain
21 of the AM signal was adjusted to control for changes in average power (5).

22

23 The animal’s contact with the spout was monitored during the final 100 msec of each trial. Breaking
24 spout contact for at least 50 msec during the monitoring window was considered a spout ‘withdrawal,’ and
25 was scored as a ‘hit’ on AM trials and as a ‘false alarm’ on non-AM trials. Behavioral performance was
26 assessed by $d' = z(HR) - z(FAR)$, where $z(HR)$ and $z(FAR)$ are the z-scores of the hit rates (HR) and
27 false alarm rates (FAR), respectively. To avoid values that approach infinity, extreme HR and FAR values
28 were set to a floor of 5% and a ceiling 95%. Behavioral testing commenced only after an animal achieved
29 a $d' \geq 2$ in a single session.

30

31 For passive sound exposure sessions, animals were placed in the test cage but did not have access
32 to a waterspout. All other elements of the experimental apparatus were identical to the detection task.
33 Sounds were presented in a manner similar to that of the task (AM stimuli randomly interspersed with 3-5
34 seconds of unmodulated noise).

35

36 Note that the fourteen animals used for the OFC electrophysiology and fiber photometry experiments
37 (Figures 2 and S1-3) were recorded from as they underwent a perceptual learning protocol in which they
38 were trained to detect progressively smaller AM depths. The details of this procedure have been
39 previously described (6). OFC’s involvement in perceptual learning will be explored in a future manuscript.

40

41 *Electrode implant procedures*

42 NeuroNexus 64-channel probes (OFC: A4x16-Poly2-5mm-20s-lin-160; auditory cortex:
43 Buzsaki64_5x12) were mounted on custom-made microdrives. The backs of the electrode shanks were
44 painted with azide-free fluorescent microspheres (FluoSpheres 0.2 μm ; ThermoFisher) just before
45 implantation. On the day before surgery, animals were placed on antibiotic treatment (minocycline in
46 drinking water; 0.02 mg/mL) and given meloxicam (1.5 mg/kg). On the day of the surgery, they were given

47 another dose of meloxicam plus dexamethasone (0.35 mg/kg). Then, they were anesthetized with
48 isoflurane (1-5%) and secured in a stereotaxic apparatus (Kopf). Ophthalmic ointment was applied to the
49 eyes and alternating swabs of alcohol and betadine were applied to the skin on the top of the head. The
50 skull was exposed and dried with hydrogen peroxide, three or four bone screws were inserted, and
51 craniotomy locations were marked over left OFC or left auditory cortex after leveling the head. Note that
52 we leveled the animal's head between lambda and bregma, rather than between lambda and the occipital
53 ridge as it was done for the gerbil brain atlas (7). Therefore, all of our rostro-caudal coordinates differ from
54 those reported in the atlas.

55 Before auditory cortex craniotomy, the temporalis muscle insertion was detached, and muscle was
56 separated from skull using dry SurgiFoam (Ethicon). The skull and screws were covered with C&B
57 Metabond (Parkell) for better implant adhesion. The edges of the craniotomy were thinned by drilling and
58 the bone flap was removed. A durotomy was made over the area of interest and electrodes were
59 implanted using the following coordinates (all relative to lambda). OFC: 1.20–1.50 mm lateral, 9.05–9.50
60 mm rostral, 2.00-2.50 mm ventral, angle=0° from vertical; implanted along coronal plane. Auditory cortex:
61 4.80 mm lateral, 3.90 mm rostral (anterior shank), 1.10-1.50 mm ventral, angle=20° clockwise from
62 vertical plane facing the animal's posterior side, implanted along parasagittal plane. A ground wire was
63 inserted into the right caudal hemisphere. Implants were secured with dental cement (Palacos). The day
64 following surgery, animals were given another dose of meloxicam and dexamethasone. Antibiotic
65 treatment continued for an additional six days. Controlled water access and behavioral experiments
66 started at least seven days after surgery.

67

68 *Electrophysiology*

69 Extracellular recordings from the OFC were obtained from freely-moving animals before (passive-
70 pre), during (task), and after (passive-post) behavioral testing sessions that took place every 24-48 hours.
71 The number of AM stimulus presentations was similar across behavioral contexts (passive-pre: $100 \pm$
72 0.10 ; task: 110 ± 3.27 ; passive-post: 99.8 ± 0.23 trials; means \pm SEMs).

73

74 Extracellular recordings from the auditory cortex were obtained before (passive-pre) and during (task)
75 behavioral testing sessions that took place every 24-48 hours. The number of AM stimulus presentations
76 was similar across behavioral contexts (passive-pre: 38.3 ± 8.08 ; task: 42.5 ± 7.05 ; means \pm SEMs).

77

78 Neurophysiological signals were obtained via one of two methods: (I) Analog signals were acquired
79 with a 64-channel wireless headstage and receiver (W64, Triangle BioSystems), preamplified and
80 digitized at 24.4 kHz sampling rate (PZ5; Tucker Davis Technologies, TDT), and integrated with
81 behavioral timestamps via RZ2 and RZ6 processors controlled by the Synapse software suite (TDT). Raw
82 signals were sent to an RS4 data streamer (TDT) and stored online. (II) Signals were preamplified and
83 digitized at 30 kHz by a 64-channel RHD headstage (Intan Technologies) connected to a slip-ring
84 commutator (Taidacent; purchased from Amazon) and integrated with behavioral timestamps using an
85 RHD recording controller (Intan) and OpenEphys software (8).

86

87 Offline signals were high-pass filtered at 150 Hz and common-median referenced across channels.
88 Multi- and single-unit sorting was performed using Kilosort2 (9). Sorting results were manually curated
89 using Phy (<https://github.com/cortex-lab/phy>). Clusters were classified as putative single-units during
90 manual curation when they presented with a high signal-to-noise ratio, clear refractory period gap in the
91 autocorrelogram and clear cross-correlogram isolation from neighboring clusters. After manual curation,
92 the Allen Brain Institute quality metrics 'presence ratio', 'amplitude cutoff fraction missing' and 'ISI
93 violation false-positive rate' (parameters: $isi_threshold = 1.5$ ms; $min_ISI = 0.15$ ms) (10) were calculated
94 (https://allensdk.readthedocs.io/en/latest/_static/examples/nb/ecephys_quality_metrics.html). We also

95 calculated the ‘refractory period violation rate’ as the percentage of interspike intervals that occurred
96 within the refractory period of 1.5 msec. Only putative single-units that had a ‘presence ratio’ > 0.9,
97 ‘amplitude cutoff fraction missing’ < 0.1, ‘ISI violation false-positive rate’ < 0.5, and ‘refractory period
98 violation rate’ < 2% were considered true single-units.

99

100 After single- and multi-unit isolation, firing rates were calculated. The window used for calculating
101 firing rates on “Hit” trials was the full 1-s AM duration. “Miss” trials produced a shock artifact, however.
102 Thus, the window used for calculating firing rates on “Miss” trials was the first 950 msec of the AM
103 stimulus. “False alarm” trials by definition do not contain an AM period, so we used a 1-s block of non-AM
104 sound during which a false alarm occurred to quantify firing rates. Peristimulus time-histograms (PSTH)
105 were generated using 10-20 msec bins.

106

107 Auditory cortical firing rates were transformed to neural d' (6, 11) using the formula:

108

$$109 \quad d' = \frac{2(\mu FR_{AM} - \mu FR_{NONAM})}{\sigma FR_{AM} + \sigma FR_{NONAM}} \quad [1]$$

110

111

112 where μFR_{AM} and μFR_{NONAM} are the mean firing rates and σFR_{AM} and σFR_{NONAM} are the standard
113 deviation of the firing rates during AM and non-AM presentations, respectively. The non-AM period used
114 for these calculations was generally the 1 s non-AM noise period immediately preceding an AM trial.
115 However, if animals withdrew from spout during that period (i.e., false alarm), the nearest previous 1 s
116 period during which the animal did not leave the spout (i.e., correct rejection) was used.

117

118 The effect of task engagement on OFC firing rates during non-AM sound presentation was assessed
119 with a Wilcoxon rank-sum test. When $p < 0.05$, the W statistic was used to determine the direction of the
120 change: ‘task-enhanced’ units exhibited a $W > 0$, while ‘task-suppressed’ units exhibited $W < 0$. The
121 magnitude of the context modulation was computed for each OFC unit using the z-score formula:

122

$$123 \quad \text{Context modulation} = \frac{\mu FR_{task} - \mu FR_{passive-pre}}{\sqrt{\text{Var}(FR_{task}) + \text{Var}(FR_{passive-pre})}} \quad [2]$$

124

125

126 where μFR_{task} and $\mu FR_{passive-pre}$ are the mean firing rates and $\text{Var}(FR_{task})$ and $\text{Var}(FR_{passive-pre})$ are
127 the firing rate variances during the task and during the passive-pre periods, respectively.

128

129 The response of OFC neurons to AM sound presentation was assessed by calculating the area under
130 the receiver operating characteristic curve (auROC) from peri-stimulus time histograms (PSTH; [Figure
131 S1A-B](#)), as previously described (12). This transformation is useful for comparing response dynamics
132 across many units with widely different firing rates. Briefly, PSTHs were generated using 10-ms bins
133 starting 2 s before until 5 s after trial onset ([Figure S1A](#)). We compared the histogram of firing rates during
134 a baseline period (from 2 to 1 s before onset) to the histogram during 100-ms windows along the entire
135 PSTH ([Figure S1C-D](#)). For these comparisons, a moving criterion vector (\vec{c}) was created ranging from 0
136 to maximum firing rate in the PSTH in 100-ms increments. For each value c in \vec{c} , we calculated the
137 probability that the activity during each bin was higher than c and plotted it against the probability that the
138 activity during baseline was higher than c , constructing an ROC curve ([Figure S1E-F](#)). The auROC was
139 calculated via trapezoidal numerical integration. AuROC values range from 0 to 1, and values above 0.5
140 indicate relative increases, while values below 0.5 indicate relative decreases in firing.

141
142 *Vector strength*

143 Phase-projected vector strength was calculated as in (13). Briefly, the standard trial-by-trial vector
144 strength (VS_t) was calculated as

$$145 \quad VS_t = \frac{\sqrt{(\sum_{i=1}^n \cos\theta_i)^2 + (\sum_{i=1}^n \sin\theta_i)^2}}{n} \quad [3]$$

147 where n is the number of spikes in a given trial and θ_i is the phase of each spike in relation to the
148 stimulus modulation period. θ_i was calculated as

$$149 \quad \theta_i = 2\pi \frac{\text{mod}(t_i, p)}{p} \quad [4]$$

152
153 where $\text{mod}(t_i, p)$ is the modulo (division remainder) between the spike time relative to the onset of the
154 stimulus t_i and the modulation period for a 5 Hz stimulus p (i.e., 0.2 s). The phase-projected vector
155 strength (VS_{pp}) was calculated as

$$156 \quad VS_{pp} = VS_t \cos(\phi_t - \phi_c) \quad [5]$$

159
160 where ϕ_t and ϕ_c are the trial-by-trial and mean phase angle, calculated as

$$161 \quad \phi = \arctan2 \frac{\sum_{i=1}^n \sin\theta_i}{\sum_{i=1}^n \cos\theta_i} \quad [6]$$

164
165 where n is the number of spikes in each trial (ϕ_t) or in all trials (ϕ_c), and $\arctan2(y/x)$ yields the angle
166 between the x-axis and the vector from $[0, 0]$ to $[x, y]$ (base R function). VS_{pp} ranges from -1 (all spikes in
167 each trial are out of phase with the mean response) to 1 (all spikes are in phase with the mean response).

169
170 *Fiber photometry*

171 Pre-operative care was as described above. The skull was exposed, dried with hydrogen peroxide,
172 and leveled between lambda and bregma. Two bone screws were inserted, and craniotomy locations
173 were marked over left OFC and left auditory cortex. The temporalis muscle was detached as described
174 above. A virus (AAVrg-syn-jGCaMP8s-WPRE; Addgene; (14)) was injected into the left auditory cortex to
175 drive retrograde expression of a genetically-encoded calcium indicator (jGCaMP8s). Injections were made
176 at three locations along the rostro-caudal axis between 2.40 and 3.90 mm rostral to lambda. At each
177 rostro-caudal location, injections were made at two depths relative to the pial surface (0.90 and 0.30 mm;
178 200 nL per depth), totaling 1200 nL. Each injection was made directly into the temporal aspect of the
179 brain, with the pipette angled 45 degrees laterally. The auditory cortex craniotomy was covered with
180 KwikSil (WPI) and the skin was repositioned to cover the craniotomy. Skin margins were glued with
181 cyanoacrylate tissue adhesive and bone screws and skull were covered with Metabond. Then, a
182 craniotomy over the left OFC was made and an optical fiber (400 μm core; $\text{\O}1.25$ mm ceramic ferrule; 0.5
183 NA; RWD Life Science) was implanted in the left OFC using the following coordinates (relative to
184 lambda): 1.2 mm lateral, 8.90-9.05 mm rostral, 2.90-3.20 mm ventral from pial surface). The craniotomy

185 was covered with KwikSil and the fiber was secured with dental cement. Post-operative care was as
186 described above. One control animal (female) was injected with AAVrg-hSyn-eGFP (Addgene) in the left
187 auditory cortex and had a fiber implanted in the left OFC as described above. Controlled water access
188 and behavioral experiments started at least three weeks after surgery to allow for virus expression. Fiber
189 photometry recordings were performed four weeks after surgery.

190

191 All optical equipment (patch cords, fluorescence MiniCube, 405 and 465 nm connectorized LEDs,
192 LED driver and Newport photoreceiver module) were purchased from Doric Lenses. LED driver control
193 and photovoltaic signal recording was sampled at 1 kHz using an RZ2 processor and Synapse software
194 (Tucker-Davis Technologies).

195

196 Fluorescence was recorded using a 465 nm LED. Calcium-independent (i.e., isosbestic) signals were
197 also recorded using a 405 nm LED to correct for movement artifacts and fluorescence decay. The
198 isosbestic point of GCaMP is ~410 nm (15).

199

200 Before each recording day, patch cords were photobleached overnight. Animal fiber-optic cannulas
201 were connected to the system using a quick-release connector (ADAL3; ThorLabs). Light intensity at the
202 tip of the animal-connecting patch cord was measured with a photodiode power sensor and energy meter
203 (S120C and PM100USB; ThorLabs). Light output (465 and 405 nm respectively) was ~90 and 28 μ W for
204 all animals except for one male (~45 and 28 μ W).

205

206 Photometry signals were processed offline similarly to (16). Briefly, 465 and 405 nm signals were 5
207 Hz low-pass filtered and smoothed with a 100-point zero-phase moving average filter. Then, LED onset
208 artifacts were removed, baseline fluctuations were corrected with the adaptive iteratively reweighted
209 Penalized Least Squares algorithm (airPLS) (17) and signals were standardized by median subtraction
210 and division by standard deviation. The standardized 405 signal was fitted to the standardized 465 signal
211 with non-negative robust linear regression and the fit was subtracted from the standardized 465 signal,
212 resulting in a dF/F signal. Finally, this resulting dF/F signal was aligned to behaviorally relevant
213 timestamps and z-scored using a baseline period ranging from 1 s before stimulus until stimulus onset.

214

215

216 *Brain cannulation and infusions*

217 Pre- and post-surgical care were as described above. The skull was exposed and dried, and two
218 bone screws were inserted. The skull and screws were covered with C&B Metabond (Parkell) for better
219 implant adhesion. Craniotomies and durotomies were performed over OFC. Double guide cannulas (26-
220 gauge, 5 mm length, 1.5 mm center-to-center distance; PlasticsOne model C235GS-5-1.2/SPC) were
221 inserted just above OFC using the following coordinates (all relative to lambda): lateral = 1.50 mm, rostral
222 = 8.75-9.05 mm, ventral = 1.50 mm; angle=0° from vertical) and secured with dental cement (Palacos).
223 Dummy cannula (33-gauge, 0.25 mm protruding from guide cannula; PlasticsOne model C235DCS-
224 5/SPC) were inserted into the guides and secured in place with a dust cap.

225

226 Starting at least seven days after surgery, animals were placed on controlled water access and
227 trained to detect AM sounds as described above. Intracortical infusions only began after animals reached
228 expert performance on the task ($d' \geq 2$). Muscimol (abcam) was dissolved in in 0.9% saline to achieve a
229 concentration of 1-2 μ g/ μ L. Infusion cannulas (33 gauge, protruding 1 mm from guide cannula;
230 PlasticsOne model C235IS-5/SPC) containing muscimol or saline were inserted into the guides. Bilateral
231 OFC infusions (0.25-0.5 μ L/hemisphere, 0.2 μ L/min rate) were made simultaneously via a six-channel
232 programmable pump (NE-1600, New Era) and 10 μ L glass syringes (Hamilton 1801). Infusions were

233 performed ~40 min before the behavioral task under light isoflurane anesthesia. The entire infusion
234 procedure lasted between 6 and 10 minutes and animals typically recovered from anesthesia within 2
235 minutes.

236

237 To estimate drug spread and cannula placement, fluororuby (Dextran, Tetramethylrhodamine, 10,000
238 MW, Lysine Fixable, Invitrogen) was diluted to 5% in sterile saline and infused through the cannulas
239 under light isoflurane anesthesia at the end of the study. Immediately after infusions animals were
240 perfused and brains were processed for histology as described below.

241

242 *Histology and imaging*

243 At the end of all experiments, animals were deeply anesthetized with a mixture of ketamine (150
244 mg/kg) and xylazine (6 mg/kg) in sterile saline and transcardially perfused first with ~20 mL of phosphate
245 buffered saline (PBS) then with ~20 mL of 4% paraformaldehyde (PFA) in phosphate buffered saline.
246 After perfusion, implants were removed, and brains were extracted and postfixed in PFA for 1-7 days until
247 sectioning. Brains were then transferred to PBS, embedded in 6% agar, and sectioned on a vibratome
248 (Leica VT-1000S) at 70 μ m thickness. Slices were collected and mounted on gelatinized slides and
249 coverslipped with ProLong Gold or Diamond mountant (Molecular Probes).

250

251 GFP-containing tissue (photometry experiment) was processed for GFP immunofluorescence for
252 signal amplification. First, free-floating sections were washed in PBS 3x10 min. Non-specific binding was
253 blocked by incubation in 10% normal goat serum (NGS) in phosphate buffered saline containing Triton-X
254 (Sigma; 0.3% PBT) for 2 h at room temperature. Following the blocking step, slices were incubated in
255 1:1000 rabbit anti-GFP primary antibody (ThermoFisher #A11122) diluted in the same blocking solution
256 (NGS + 0.3% PBT) for 1 h at room temperature then 40-48 h at 4° C. Following primary incubation, slices
257 were washed in 0.1% PBT 3x15 min then incubated in 1:1000 goat anti-rabbit Alexa-488 secondary
258 antibody (ThermoFisher #A32731) for 1 h at room temperature. Finally, following secondary incubation,
259 slices were washed in 0.1% PBT 3x10 min and coverslipped with ProLong Diamond.

260

261 Sections were imaged either via epifluorescence (Leica DM750) or confocal microscopy (Zeiss LSM
262 980 Airyscan 2) at 10x magnification. For epifluorescence images, tiles were taken manually and stitched
263 together using Photoshop 2023 panorama PhotoMerge function (Adobe).

264

265 *Software and analysis*

266 We used the ePsych software developed by Dr. Daniel Stolzberg (<https://github.com/dstolz/epsych>)
267 for MatLab R2014a (MathWorks) for behavioral data acquisition and control.

268

269 All data were processed offline by custom MatLab pipelines ([https://github.com/caraslab/caraslab-](https://github.com/caraslab/caraslab-behavior-analysis)
270 [behavior-analysis](https://github.com/caraslab/caraslab-behavior-analysis), <https://github.com/caraslab/caraslab-spikesortingKS2>, and
271 <https://github.com/caraslab/caraslab-fiberphotometry>), then further analyzed by custom Python and R
272 routines (available upon request).

273

274 Statistical analyses were performed by generalized linear models followed by ANOVA (GLM/ANOVA)
275 using the 'glmmTMB' (18) and the 'car' (19) packages for R. Normality of GLM residuals was assessed
276 after each fit by visually inspecting the distribution of studentized residuals (q-q plots) using the
277 'DHARMA' package for R (20). When normality was not fulfilled, data were square-root- or log-
278 transformed, and GLMs were rerun. Before transformation, data containing negative numbers were
279 rescaled using the formula $F(x) = x + 2|\min(\vec{X})|$, where x represents an individual value and $\min(\vec{X})$

280 represents the lowest value in the dataset. When interactions were significant, Bonferroni multiple
281 comparison post-hoc tests using the package 'emmeans' for R (<https://github.com/rvlenth/emmeans>)
282 were used after "regridding" the data into original units if a transformation was required.

283

284 All GLM fixed effects can be found in the statistical tables. GLM random effects were as follows. The
285 effect of behavioral context on OFC activity included Unit nested under Subject (Figure 2F) or Context
286 (passive-pre, task, passive-post) nested under Unit nested under Subject as random effects (Figure 2G
287 and S3C). The effect of OFC suppression on behavioral AM detection included Subject as random effect
288 (Figures 3C-H, 4C and S4-5). The effect of behavioral context on auditory cortical activity was separately
289 analyzed for each drug treatment (saline or muscimol) including Context (passive, task) nested under Unit
290 nested under Subject as random effects (Figure 4E-H and S6), or Unit nested under either Behavioral d'
291 (Figure 5B) or performance (good vs poor, Figure 5C) nested under Subject as random effects. All
292 supplementary statistical results can be found in Table S1.

SI References

1. M. L. Caras, D. H. Sanes, Sustained perceptual deficits from transient sensory deprivation. *Journal of Neuroscience* **35**, 10831–10842 (2015).
2. E. C. Sarro, G. Von Trapp, T. M. Mowery, V. C. Kotak, D. H. Sanes, Cortical Synaptic Inhibition Declines during Auditory Learning. *J. Neurosci.* **35**, 6318–6325 (2015).
3. E. C. Sarro, D. H. Sanes, Prolonged maturation of auditory perception and learning in gerbils. *Devel Neurobio* **70**, 636–648 (2010).
4. E. C. Sarro, D. H. Sanes, The Cost and Benefit of Juvenile Training on Adult Perceptual Skill. *J. Neurosci.* **31**, 5383–5391 (2011).
5. N. F. Viemeister, Temporal modulation transfer functions based upon modulation thresholds. *The Journal of the Acoustical Society of America* **66**, 1364–1380 (1979).
6. M. L. Caras, D. H. Sanes, Top-down modulation of sensory cortex gates perceptual learning. *Proceedings of the National Academy of Sciences of the United States of America* **114**, 9972–9977 (2017).
7. S. Radtke-Schuller, *et al.*, Brain atlas of the Mongolian gerbil (*Meriones unguiculatus*) in CT/MRI-aided stereotaxic coordinates. *Brain Structure and Function* **221** (2016).
8. J. H. Siegle, *et al.*, Open Ephys: an open-source, plugin-based platform for multichannel electrophysiology. *J. Neural Eng.* **14**, 045003 (2017).
9. M. Pachitariu, S. Sridhar, C. Stringer, Solving the spike sorting problem with Kilosort. *bioRxiv* (2023).
10. D. N. Hill, S. B. Mehta, D. Kleinfeld, Quality metrics to accompany spike sorting of extracellular signals. *Journal of Neuroscience* **31**, 8699–8705 (2011).
11. G. von Trapp, B. N. Buran, K. Sen, M. N. Semple, D. H. Sanes, A decline in response variability improves neural signal detection during auditory task performance. *Journal of Neuroscience* **36**, 11097–11106 (2016).
12. J. Y. Cohen, S. Haesler, L. Vong, B. B. Lowell, N. Uchida, Neuron-type-specific signals for reward and punishment in the ventral tegmental area. *Nature* **482**, 85–88 (2012).
13. P. Yin, J. S. Johnson, K. N. O'Connor, M. L. Sutter, Coding of Amplitude Modulation in Primary Auditory Cortex. *Journal of Neurophysiology* **105**, 582–600 (2011).
14. Y. Zhang, *et al.*, Fast and sensitive GCaMP calcium indicators for imaging neural populations. *Nature* **615**, 884–891 (2023).
15. C. K. Kim, *et al.*, Simultaneous fast measurement of circuit dynamics at multiple sites across the mammalian brain. *Nature Methods* **13**, 325–328 (2016).
16. E. Martianova, S. Aronson, C. D. Proulx, Multi-fiber photometry to record neural activity in freely-moving animals. *Journal of Visualized Experiments* **2019**, 1–9 (2019).
17. Z. M. Zhang, S. Chen, Y. Z. Liang, Baseline correction using adaptive iteratively reweighted penalized least squares. *Analyst* **135**, 1138–1146 (2010).
18. M. Brooks E., *et al.*, glmmTMB Balances Speed and Flexibility Among Packages for Zero-inflated Generalized Linear Mixed Modeling. *The R Journal* **9**, 378–400 (2017).
19. F. John, S. Weisberg, *An R Companion to Applied Regression*, 3rd Ed. (Sage Publications, 2019).
20. F. Hartig, DHARMA: Residual Diagnostics for Hierarchical (Multi-Level / Mixed) Regression Models (2021).

Supplementary figures and tables

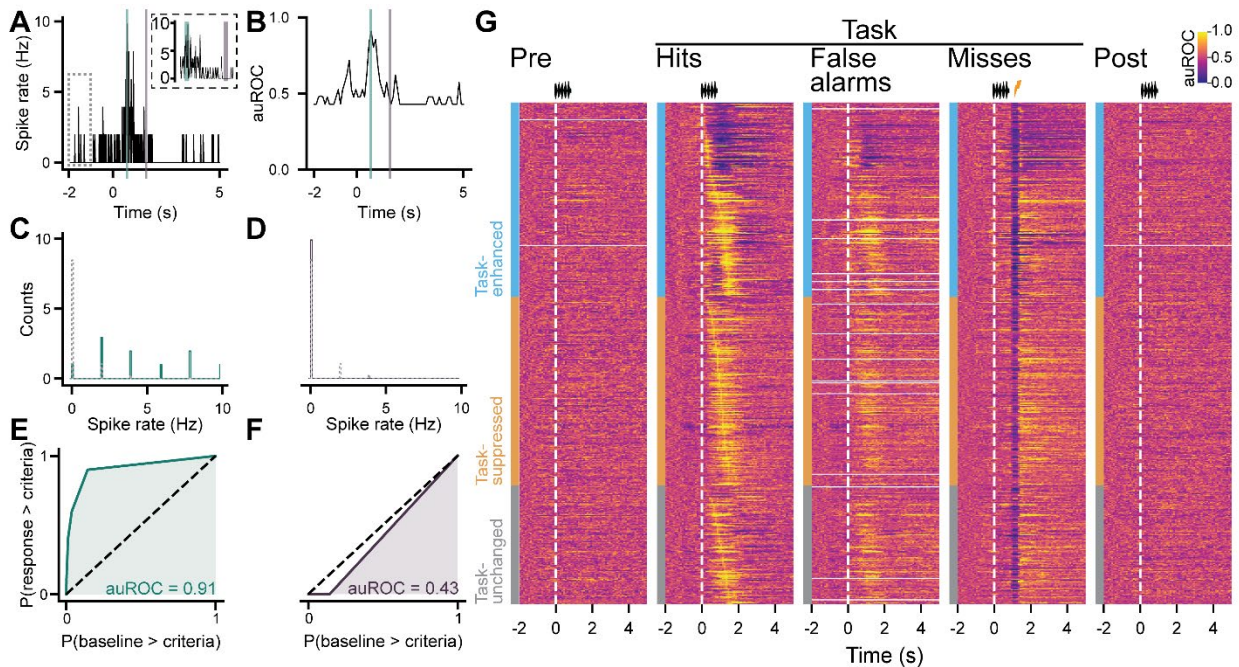


Figure S1. OFC neurons exhibit heterogeneous firing rate changes during sound-guided behavior. (A-B) Peri-stimulus time histograms (PSTH) around trials (A) were used to generate normalized firing rate auROC PSTHs (B). We compared the spike rate during a baseline period (dashed gray box) to the spike rate during 100-ms windows along the entire PSTH. Two example windows are shown in green and purple. Inset in A represents a magnified view around the windows to illustrate that each 100-ms window contains 10x 10-ms spike rate values. (C-D) Count histograms illustrating the spike rate bins during baseline period (dashed lines) and during the 100-ms example windows (green and purple solid lines) from the PSTH illustrated in A. Spike rate distributions were compared using a criterion vector (see Supplementary Methods for details) constructing ROCs (E-F), from which auROCs could be calculated. (G) Heatmaps illustrate normalized neuronal firing (auROC) aligned to trial onset (Time = 0 s; vertical dashed white lines). Units (rows) are separated by the type of modulation exhibited during non-AM sound presentation (task-enhanced, -suppressed or -unchanged as in Figure 2). Rows are ordered by time of the maximum absolute auROC change since AM trial onset during Hit trials, and the same order is used across other trial types. False alarm trials by definition do not contain an AM period, so Time = 0 s represents the onset of a 1-s trial block within which false alarms occurred. Data are from 298 single- and 227 multi-units. Solid white rows are from sessions during which auROC could not be calculated due to spikes not occurring that period.

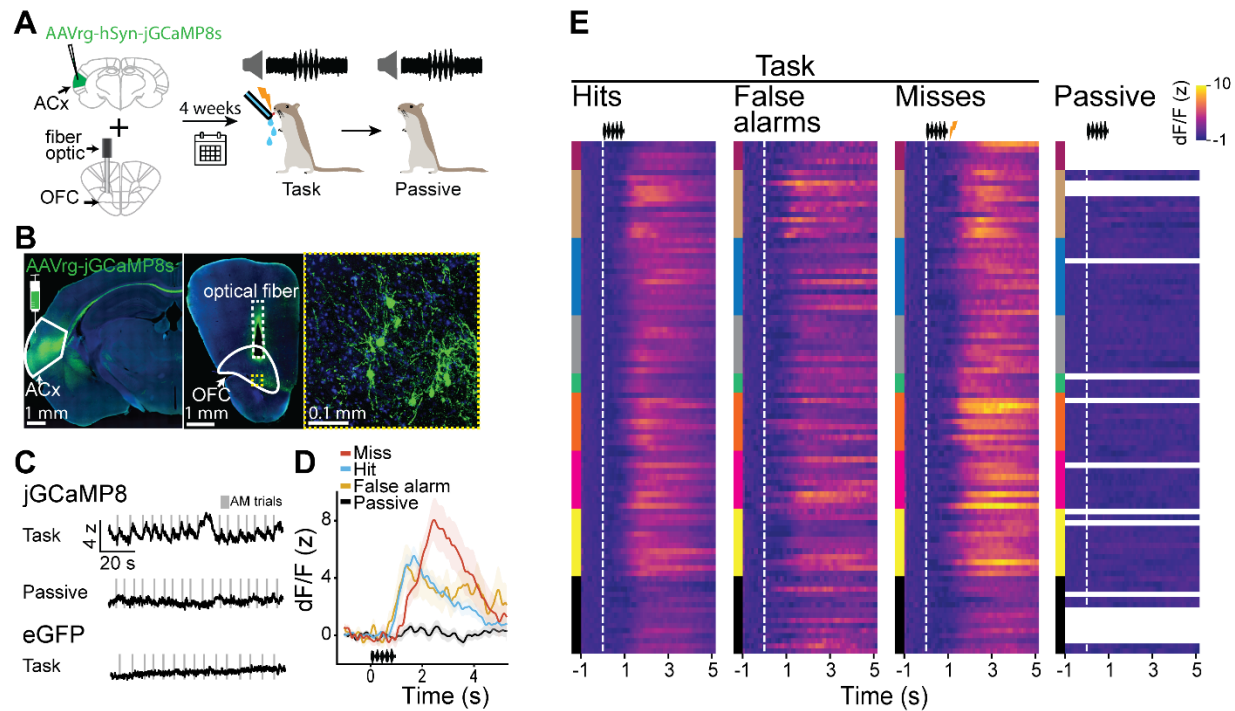


Figure S2. OFC neurons that innervate auditory cortex show increased trial-based activity during task performance. (A) Calcium transients from OFC neurons that project to auditory were recorded via fiber photometry in nine animals (four females). Auditory cortex was injected with a virus retrogradely-expressing jGCaMP8s and an optical fiber was implanted in left OFC. After four weeks to allow for virus expression, animals were placed on controlled water access and tested on the AM detection task. Photometry signals were collected during the task and during a period of passive sound exposure immediately following the task. (B) Virus injection site in auditory cortex (left) and fiber location in OFC (middle and right) were confirmed after the experiment. (C) Calcium transients time-locked to AM trials were only evident during task engagement (top) and not during passive sound exposure (middle). To confirm that the recorded signals were not related to movement artifacts, one female was injected with a virus retrogradely-expressing enhanced green fluorescent protein (eGFP) and a fiber optic was placed in OFC. No task-related transients were detected in this animal (bottom). (D) Representative mean \pm standard error calcium transients from one recording session demonstrating calcium dynamics around behavioral responses and not during passive AM presentation. (E) Heatmaps illustrate calcium dynamics around behavioral responses and AM presentations during task and passive periods. Responses were aligned to trial onset (Time = 0 s; vertical dashed white lines). False alarm trials by definition do not contain an AM period, so Time = 0 s represents the onset of a 1-s trial block within which false alarms occurred. Each row represents one session. Vertical color bars represent sessions from the same animal. Since calcium transients were not evident during passive sound playback, recordings were not performed for every session. Blank rows in the passive session columns represent sessions in which no passive recording was made.

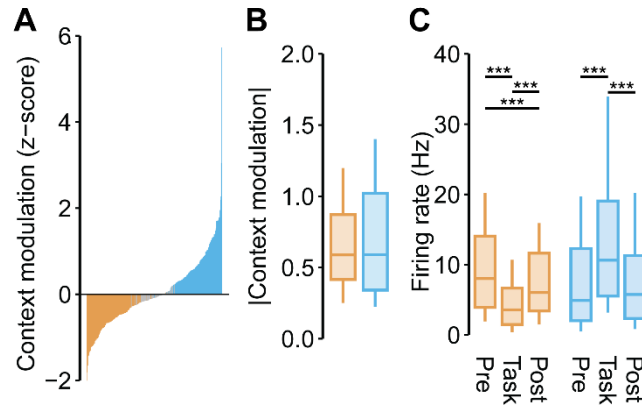


Figure S3. Context-dependent dynamics in non-AM firing are present even when the analysis is restricted to single-units. Same analysis as in Figure 2E-G but restricted to single-units ($n = 117$ task-enhanced and $n = 116$ task-suppressed out of 298 single-units). (A) Context modulation values are presented for all single-units sorted in increasing order. Gray bars represent units without significant context modulation. (B) Absolute modulation magnitudes were similar between task-enhanced and -suppressed single-units. (C) Task-suppressed single-units exhibited reductions in tonic activity that persisted in the passive-post period. The activity of task-enhanced single-units, on the other hand, returned to passive-pre levels after the task ended. *** $p < 0.001$

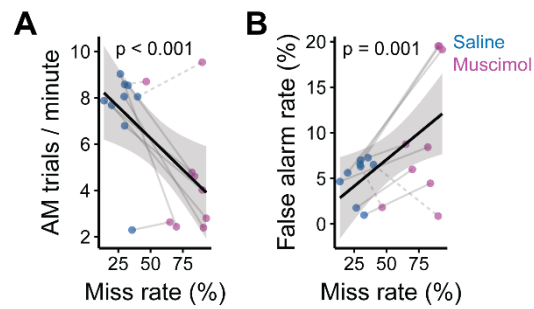


Figure S4. Slower trial completion and increased false alarm rates during OFC inactivation may be explained by the increased frequency of punishment. (A) The number of AM trials completed per minute negatively correlates with the miss rate. (B) The false alarm rate positively correlates with the miss rate. Blue dots represent days when animals received saline infusions into OFC, while magenta dots represent days when animals received muscimol infusions. Gray lines connect data from the same animal. Dashed lines indicate animals that received unilateral left OFC infusions due to partially clogged cannulas.

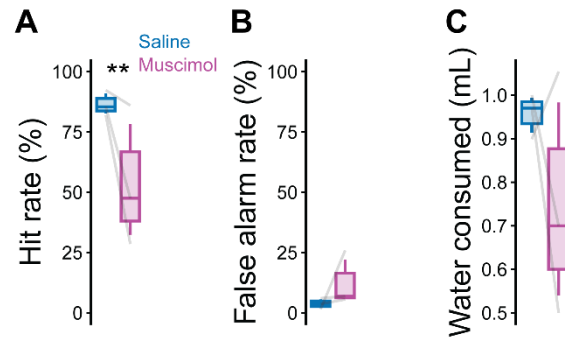


Figure S5. The behavioral effects of OFC suppression replicate in animals with chronic electrode implants in the auditory cortex. OFC suppression significantly reduced behavioral hit rates (A) but did not significantly affect false alarm rates (B) or water consumed during the task (C). ** $p < 0.01$.

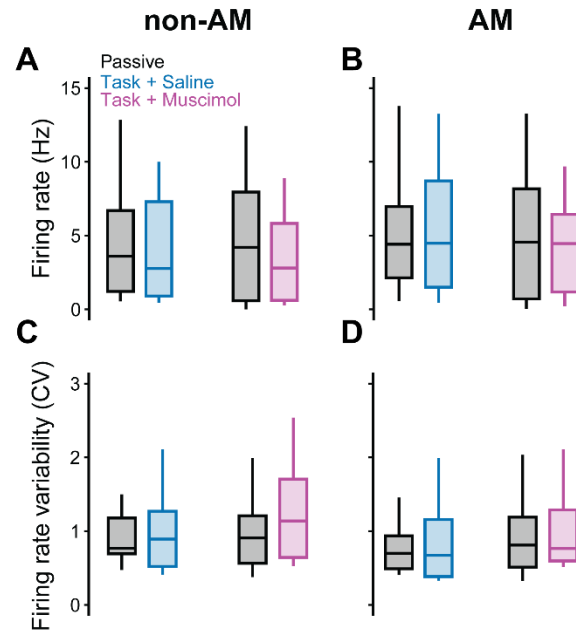


Figure S6. Effects of OFC suppression on auditory cortical firing rates and firing rate variability. (A-B) Neither task engagement nor OFC suppression systematically affect non-AM (A) or AM firing rates (B) of auditory cortical single- and multi-units. (C-D) Neither task engagement nor OFC suppression systematically affect non-AM (C) or AM firing rate variability (D).

Table S1. Statistical results

Figure	Test	Factor(s)	Statistic	P value
S3B	GLM/ANOVA	Type	$\chi^2_1 = 1.023$	0.312
S3C	GLM/ANOVA: Task-suppressed	Session	$\chi^2_2 = 218.340$	< 0.001
		Bonferroni: Task-suppressed	Pre – Task	$t_{341} = 14.515$
		Pre – Post	$t_{341} = 4.861$	< 0.001
		Task – Post	$t_{341} = -9.654$	< 0.001
	GLM/ANOVA: Task-enhanced	Session	$\chi^2_2 = 189.980$	< 0.001
		Bonferroni: Task-enhanced	Pre – Task	$t_{345} = -10.914$
		Pre – Post	$t_{345} = -1.248$	0.563
		Task – Post	$t_{345} = 10.075$	< 0.001
S4A	GLM/ANOVA	Miss rate	$\chi^2_1 = 15.630$	< 0.001
S4B	GLM/ANOVA	Miss rate	$\chi^2_1 = 10.778$	0.001
S5A	GLM/ANOVA	Treatment	$\chi^2_1 = 8.271$	0.004
S5B	GLM/ANOVA	Treatment	$\chi^2_1 = 2.715$	0.099
S5C	GLM/ANOVA	Treatment	$\chi^2_1 = 2.323$	0.127
S6A	GLM/ANOVA: Saline	Context	$\chi^2_1 = 0.678$	0.410
	GLM/ANOVA: Muscimol	Context	$\chi^2_1 = 1.900$	0.168
S6B	GLM/ANOVA: Saline	Context	$\chi^2_1 < 0.001$	0.998
	GLM/ANOVA: Muscimol	Context	$\chi^2_1 = 0.214$	0.643
S6C	GLM/ANOVA: Saline	Context	$\chi^2_1 = 0.223$	0.637
	GLM/ANOVA: Muscimol	Context	$\chi^2_1 = 0.122$	0.726
S6D	GLM/ANOVA: Saline	Context	$\chi^2_1 = 0.003$	0.959
	GLM/ANOVA: Muscimol	Context	$\chi^2_1 = 0.546$	0.460